*CRYSTALLOGRAPHY REPORTS, 2025, Vol. 70, No. 1, pp. 3–9*

## CRYSTAL CHEMISTRY

# SIMULATION OF $ZnWO_4$ SANMARTINITE BY THE METHOD OF INTERATOMIC POTENTIALS

**© 2025 V. B. Dudnikova[a,*], E. V. Zharikov[b], and N. N. Eremin[a,c]**

[a] *Lomonosov Moscow State University, Moscow, Russia*
[b] *Prokhorov General Physics Institute of the Russian Academy of Sciences, Moscow, Russia*
[c] *Institute of Geology of Ore Deposits, Petrography, Mineralogy and Geochemistry, Moscow, Russia*
**e-mail: VDudnikova@hotmail.com*

Received October 07, 2024
Revised November 15, 2024
Accepted November 15, 2024

**Abstract.** The structure and properties of $ZnWO_4$ have been simulated using the method of empirical interatomic potentials. The system of consistent interatomic potentials has been developed, which makes it possible to describe the structure, elastic and thermodynamic properties of zinc tungstate and provide the simulation of more complex composite media involving this component.

**DOI:** 10.31857/S00234761250101e1

## INTRODUCTION

The mineral sanmartinite $ZnWO_4$ was first discovered in 1948 near San Martín, Argentina, and immediately attracted researchers' attention as a promising luminescent material [1]. It continues to be actively studied today, finding new applications.

$ZnWO_4$ undergoes congruent melting at 1216 ± 5°C [2] and does not experience polymorphic phase transitions below its melting point. Therefore, large $ZnWO_4$ crystals can be grown directly from the melt using the conventional Czochralski method [3–5]. $ZnWO_4$ crystals as large as 14 kg have been obtained [6]. Recent developments have made it possible to produce high-quality, large-volume zinc tungstate scintillator crystals with extremely low levels of radioactive contamination [7, 8].

Zinc tungstate is a multifunctional, non-toxic material with several unique properties, including a high refractive index, thermal and chemical stability, a high X-ray absorption coefficient, and a light yield higher than that of commercial $Bi_4Ge_3O_{12}$. It also boasts high density, short decay times, and low afterglow in luminescence [8–10]. Due to these properties, zinc tungstate is widely used as a scintillator [11], photocatalyst [12], and phosphor [13]. $ZnWO_4$ crystals are classified as anisotropic scintillators, exhibiting anisotropy in light output for heavy particles (protons, α-particles) as opposed to an isotropic response to β- and γ-radiation [14]. Consequently, zinc tungstate is of significant interest for researchers involved in double beta decay searches, dark matter detection, and cryogenic experiments aimed at identifying rare α- and β-decays [15].

Zinc tungstate crystals are effective nonlinear media and are utilized in the development of lasers based on stimulated Raman scattering [16]. $ZnWO_4$-based phosphors doped with rare-earth elements play a crucial role in the creation of solid-state lasers emitting at various wavelengths [17, 18], as well as in the production of white LEDs for solid-state lighting applications [19, 20].

$ZnWO_4$ has a wolframite-type structure (monoclinic symmetry, space group $P2/c$) with two formula units per unit cell [21, 22]. The structure of $ZnWO_4$ is depicted in Fig. 1. Zinc and tungsten ions are coordinated octahedrally by oxygen (Fig. 1a). The $ZnO_6$ octahedron consists of two $O_1$ atoms and four $O_2$ atoms, while the $WO_6$ octahedron includes four $O_1$ atoms and two $O_2$ atoms. The structure comprises alternating layers of zigzag chains of $ZnO_6$ octahedra sharing edges and $WO_6$ octahedra also sharing edges, extending infinitely along the [001] direction (Fig. 1b). Each $ZnO_6$ octahedral chain is connected through shared oxygen vertices to four $WO_6$ octahedral chains, and vice versa, forming open channels along the [001] direction (Fig. 1a).

The structural and property simulation of zinc tungstate has been conducted *ab initio* in several studies using density functional theory (**DFT**) [23–26], employing various approaches. For example, in [23], to compute elastic constants and moduli, two now-standard numerical approximations were used to calculate exchange-correlation energy: the local-density approximation (**LDA**) [27] and the generalized gradient approximation (**GGA**) [28]. It was noted that GGA better describes inhomogeneous systems, particularly those with covalent bonding. In [24, 25], the generalized

gradient approximation (GGA) with the widely-used Perdew–Burke–Ernzerhof (**PBE**) functional was employed to describe the exchange-correlation potential [29]. In contrast to previous studies, [26] applied the DFT method using a linear combination of atomic orbitals (**LCAO**).

An alternative to *ab initio* calculations is atomistic simulation using empirical interatomic potentials, which has been successfully applied to describe various systems, including molybdates and tungstates, their solid solutions, intrinsic and impurity defects, and the local environments of matrix and activator ions (e.g., [30–35]). However, sanmartinite $ZnWO_4$ has not been studied using the interatomic potential method.

This study focuses on developing a potential system within atomistic simulation that would describe the properties of $ZnWO_4$ and enable simulations involving this component in more complex systems, which are increasingly being applied [17–20, 36–39].

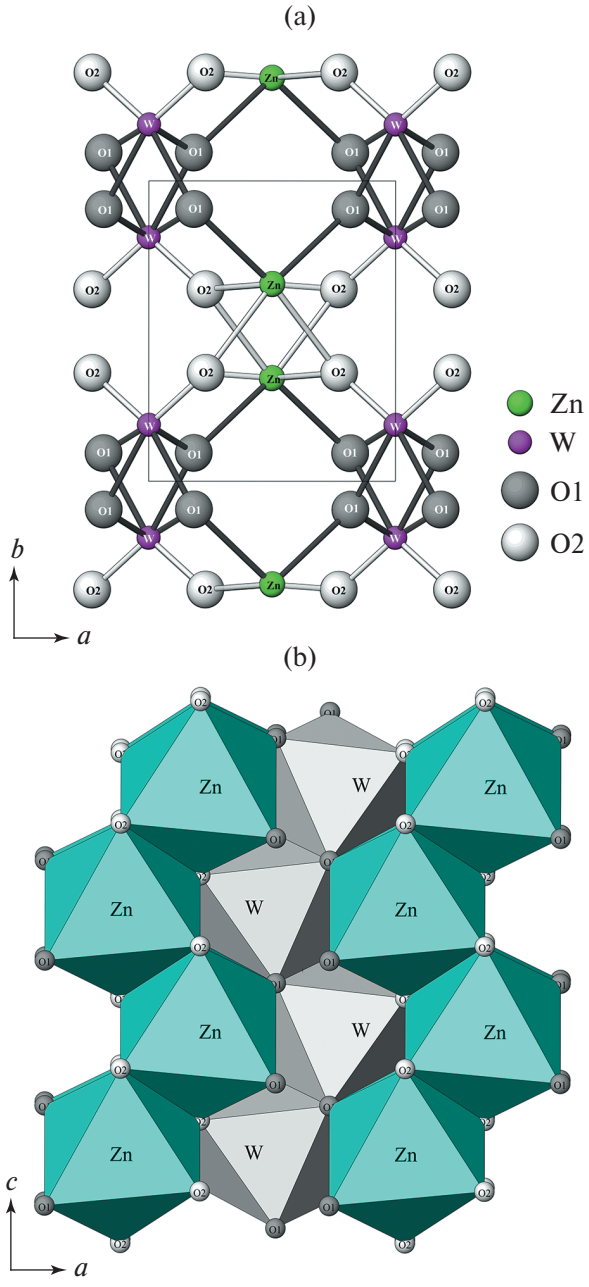


**Fig. 1.** Structure of zinc tungstate $ZnWO_4$, projection onto the plane: a – *ab*, b – *ac*.

## SIMULATION METHODOLOGY

Simulation was conducted using the interatomic potentials method with the GULP 4.0.1 (General Utility Lattice Program) software [40], which is based on minimizing the energy of interatomic interactions.

The atomistic approach relies on empirically determined potentials that describe interactions between ions in the crystal. The pair potential $U_{ij}$ for ions $i$ and $j$ with charges $q_i$ and $q_j$ was defined as follows:

$$U_{ij}\left(R_{ij}\right) = q_i q_j e^2 / R_{ij} + A_{ij} \exp\left(-R_{ij}/\rho_{ij}\right) - C_{ij}/R_{ij}^6, \quad (1)$$

where $R_{ij}$ is the interatomic distance, $A_{ij}$, $\rho_{ij}$, $C_{ij}$ are empirical parameters of short-range potentials. In this study, the interaction range was set at 15 Å for oxygen-oxygen contacts and 12 Å for other contacts. The covalent nature of the bonding was accounted for by introducing the effective charge of the ions.

The initial model adopted the structure of $ZnWO_4$ with cell parameters and atomic coordinates according to [22]. For zinc, a charge of 1.26 *e* was used, as in ZnO [41]. The charges for tungsten and oxygen were varied. The potential parameters for $ZnWO_4$ were determined through an iterative "fitting relax" procedure [40], under isotropic changes in the unit cell parameters.

## DISCUSSION OF RESULTS

The best agreement with experimental values for unit cell parameters and atomic coordinates of $ZnWO_4$ was achieved using the atomic charges and interatomic potential parameters listed in Table 1. These parameters were used to determine a range of properties of zinc tungstate. The results are presented in Tables 2–5, compared with existing literature data.

Table 2 shows the unit cell parameters, cell volume, and atomic coordinates. The structure of $ZnWO_4$ has been studied in many works with varying levels of reliability and accuracy. The most precise, detailed, and reliable experimental data from three studies [22, 42, 43] are provided in Table 2. As can be seen, the results from these studies are in good agreement, as are the simulation results from this study. The unit cell parameters and volume reproduce the experimental data with an accuracy within tenths of a percent. In most cases, atomic positions are localized quite accurately

(the deviations of atomic coordinates from experimental values do not exceed 5%). The least accurately determined positions are those of oxygen atoms along the *x*-axis, which likely contributes the most to the error in determining interatomic distances.

Table 3 presents a comparison of calculated interatomic distances with experimental data. For the $ZnO_6$ and $WO_6$ octahedra, the Zn–O and W–O bond pairs are shown. Additionally, the average bond lengths within the octahedra ($R_{av}$) — which determine the size of the polyhedron — and the bond length dispersion ($\Delta R$) — the difference between the largest and smallest bond lengths, characterizing the degree of polyhedral distortion — were evaluated. The greatest deviations from experimental values were observed for the Zn–O1 and W–O2 bond lengths, while the other distances agreed well with experimental results, particularly considering the variability of experimental data reported in different studies. According to the simulation results, as well as experimental data, the $ZnO_6$ octahedron is larger than the $WO_6$ octahedron (with a higher $R_{av}$). However, the $WO_6$ octahedron is more distorted (with a higher $\Delta R$). Thus, the simulation results for $ZnWO_4$ provide a good description of the structural characteristics of this compound.

Tables 4 and 5 present the results of assessing the elastic properties of $ZnWO_4$ in comparison with literature data. Table 4 lists the elastic constants ($C_{ij}$).

**Table 1.** Parameters of interatomic interaction potentials obtained in the work

| Interaction | Potential parameters | | | Atom | Charge, *e* |
|---|---|---|---|---|---|
| | *A*, eV | ρ, Å | *c*, eV·Å$^6$ | | |
| Zn–O | 98686.612014 | 0.171609 | 0.0 | Zn | 1.26 |
| W–O | 1005.782073 | 0.352777 | 0.0 | W | 5.1 |
| O–O | 2433.647679 | 0.269041 | 49.853817 | O | –1.59 |

**Table 2.** Unit cell parameters and atomic coordinates in comparison with experimental data

| Parameters, coordinates | This work | [42] | [43] | [22] |
|---|---|---|---|---|
| *a*, Å | 4.6806 | 4.69263(5) | 4.6986(8) | 4.6902(1) |
| *b*, Å | 5.7052 | 5.72129(7) | 5.7293(8) | 5.7169(1) |
| *c*, Å | 4.9167 | 4.92805(5) | 4.9367(11) | 4.9268(1) |
| β, degrees | 90.626 | 90.6321(9) | 90.615(25) | 90.626(1) |
| *V*, Å$^3$ | 131.29 | 132.300(2) | 132.89(4) | 132.14(1) |
| Zn *y*/*b* | 0.6563 | 0.6833(4) | 0.6840(2) | 0.6838(4) |
| W *y*/*b* | 0.1876 | 0.1823(5) | 0.18258(6) | 0.1820(4) |
| O1 *x*/*a* | 0.1825 | 0.2171(3) | 0.2169(10) | 0.2171(3) |
| O1 *y*/*b* | 0.9056 | 0.8955(3) | 0.1051(9) | 0.8953(2) |
| O1 *z*/*c* | 0.4499 | 0.4360(3) | –0.0637(9) | 0.4373(3) |
| O2 *x*/*a* | 0.2299 | 0.2547(3) | 0.2565(10) | 0.2557(3) |
| O2 *y*/*b* | 0.3604 | 0.3772(3) | 0.3777(10) | 0.3751(3) |
| O2 *z*/*c* | 0.3902 | 0.4005(3) | 0.3996(10) | 0.3999(3) |

**Table 3.** Interatomic distances in $ZnO_6$ and $WO_6$ octahedra

| Distances | This work | [42] | [43] | [22] | [44] | [45] | [46] |
|---|---|---|---|---|---|---|---|
| Zn–O1, Å | 2.286 | 2.026(2) | 2.025(5) | 2.025(2) | 2.0606 | | |
| Zn–O2, Å | 2.165<br>2.223 | 2.090(2)<br>2.227(3) | 2.094(5)<br>2.226(5) | 2.088(1)<br>2.234(2) | 2.1387<br>2.1326 | | |
| $R_{av}$ | 2.225 | 2.114 | 2.115 | 2.115 | 2.209 | | |
| $\Delta R$ | 0.122 | 0.201 | 0.201 | 0.209 | 0.078 | | |
| W–O1, Å | 1.794<br>2.065 | 1.915(2)<br>2.133(3) | 1.915(5)<br>2.140(5) | 1.908(1)<br>2.134(2) | 1.8554<br>2.1838 | 1.84(1)<br>2.13(1) | 1.8938<br>2.0310 |
| W–O2, Å | 1.609 | 1.790(2) | 1.797(5) | 1.784(2) | 1.8156 | 1.84(1) | 1.8370 |
| $R_{av}$ | 1.823 | 1.946 | 1.951 | 1.942 | 1.952 | 1.936 | 1.920 |
| $\Delta R$ | 0.456 | 0.343 | 0.343 | 0.350 | 0.368 | 0.29 | 0.194 |

**Table 4.** Elastic constants of $ZnWO_4$

| $C_{ij}$ | This work | Experiment | Calculation | | |
|---|---|---|---|---|---|
| | | [47] | [23]<br>DFT–LDA | [23]<br>DFT–GGA | [24]<br>DFT–GGA + PBE |
| $C_{11}$ | 198.65 | 240.23 | 252.25 | 196.88 | 199.1 |
| $C_{22}$ | 164.54 | 214.93 | 233.91 | 150.88 | 164.7 |
| $C_{33}$ | 317.72 | 287.96 | 314.59 | 258.50 | 247.8 |
| $C_{44}$ | 70.58 | 69.65 | 77.51 | 63.65 | 53.97 |
| $C_{55}$ | 118.79 | 70.01 | 94.96 | 65.27 | 61.3 |
| $C_{66}$ | 84.67 | 24.93 | 39.49 | 12.73 | 15.2 |
| $C_{12}$ | 108.34 | 108.94 | 125.17 | 75.91 | 89.98 |
| $C_{13}$ | 142.46 | 102.21 | 123.68 | 94.09 | 104.96 |
| $C_{15}$ | 28.80 | | 16.04 | 16.04 | 13.10 |
| $C_{23}$ | 66.82 | 112.99 | 122.46 | 93.80 | 93.7 |
| $C_{25}$ | 6.74 | | 13.12 | 19.65 | 3.89 |
| $C_{35}$ | 76.87 | | 15.03 | 6.49 | 11.3 |
| $C_{46}$ | –24.27 | | –7.93 | 1.11 | 8.55 |

**Table 5.** Elastic modules of $ZnWO_4$

| Modules | | This work | Experiment | | Calculation | | Calculation method |
|---|---|---|---|---|---|---|---|
| $K$, GPa | | 136.66 | 153 | [47] | 179.03 ± 1.94 | [23] | DFT–LDA |
| | | | | | 125.75 ± 5.25 | | DFT–GGA |
| | | | 161(3) | [22] | 102.37 | [24] | DFT–GGA + PBE |
| | | | | | 140 | [25] | DFT–GGA + PBE |
| | | | 145(6) | [48] | 257 | [26] | DFT–LCAO |
| $G$, GPa | | 69.03 | $G_z$ = 69.86 | [47] | – | | – |
| $E_i$, GPa | x | 93.95 | 176 | | 171.23 | [23] | DFT–LDA |
| | | | | | 146.80 | | DFT–GGA |
| | y | 104.52 | 147 | | 156.98 | | DFT–LDA |
| | | | | | 103.15 | | DFT–GGA |
| | z | 187.59 | 217 | | 231.93 | | DFT–LDA |
| | | | 183 ± 21 | [49] | 185.41 | | DFT–GGA |

The elastic properties of zinc tungstate have been relatively underexplored. There is only one experimental study from 1988 [47], where the elastic constants of $ZnWO_4$ were determined via ultrasonic phase velocity measurements. In [47], the estimation of $C_{ij}$ was conducted under the approximation of orthorhombic symmetry, resulting in an incomplete set of elastic constants (Table 4). A complete matrix has not yet been determined experimentally.

Regarding the simulation of elastic constants of zinc tungstate, they were evaluated in [23–26] using various first-principles simulation approaches. It is evident that there is a significant spread in the results, with the largest deviation observed in simulations using the DFT–LCAO method [26].

Table 5 presents the elastic moduli: bulk modulus $K$, shear modulus $G$ and Young's modulus $E_i$. The bulk and shear moduli are given according to the Hill approximation. Young's modulus indicates the anisotropy of elastic properties. $ZnWO_4$ exhibits the highest elasticity along the [001] direction, which coincides with the direction of open channels in its structure. Table 5 also includes literature data on elastic moduli. Experimental results for the bulk modulus were obtained in [22, 47, 48] using various methods. In [47], as mentioned earlier, the bulk modulus of zinc tungstate was determined based on the speed of ultrasound propagation in crystals. In [22], the bulk modulus was estimated from a neutron diffraction experiment examining the temperature dependence of $ZnWO_4$ lattice parameters, while in [48], assessments were based on an X-ray diffraction experiment determining $ZnWO_4$ lattice parameters under applied pressure. In [49], resonance methods based on laser Doppler vibrometry were used to obtain data on Young's modulus for $ZnWO_4$ nanowires. The crystals were grown along the [001] direction, with lengths of several hundred micrometers and thicknesses ranging from 67 to 120 nm. The value presented in the table refers to the maximum diameter of the nanocrystals and should correspond to values for bulk single crystals, making it comparable to other results. The calculated literature values of elastic moduli are provided in Table 5, along with the respective calculation methods.

A notable feature is the significant discrepancy among the literature data regarding the elastic properties of $ZnWO_4$. For instance, estimates of elastic constants can differ by more than 100%. The values of the bulk modulus vary from 102 to 257 GPa, while differences in Young's modulus in some cases exceed 50%. The results of interatomic potential simulation generally fall within the range defined by the literature data or are comparable to them.

Fig. 2 presents the results of simulation the temperature dependence of the heat capacity at constant volume $C_v$ compared to experimental data for the heat capacity at constant pressure $C_p$. Data from studies on the variation of $C_p$ in the range of 5–520 K [50], 5–550 K [51], and 81–301 K [52] align well with each other, almost merging due to the closeness of their values, making them difficult to distinguish in Fig. 2. The figure shows good agreement between the simulation results and experimental estimates, especially since $C_p$ is typically slightly higher than $C_v$. However, the results from [16] in the range of 293–573 K (shown by the dashed line), which indicate a significant, nearly linear

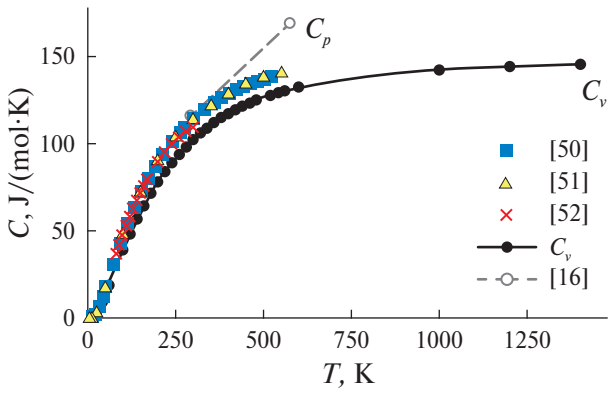


**Fig. 2.** Temperature dependence of the heat capacity of $ZnWO_4$: $C_v$ – this work, $C_p$ – [50–52], [16] (dashed line).

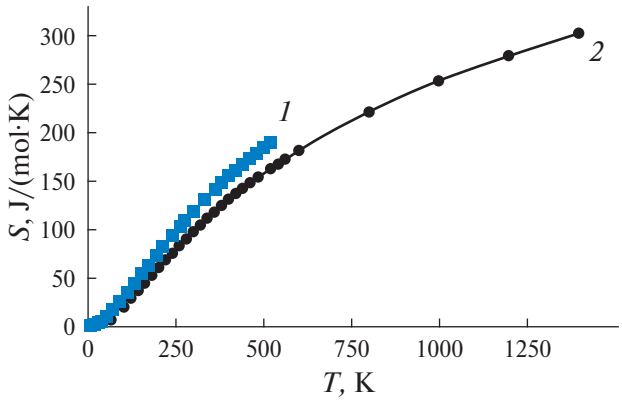


**Fig. 3.** Temperature dependence of the entropy of $ZnWO_4$: *1* – [50], *2* – this work.

increase in heat capacity in this range, are not confirmed by the simulation results. Fig. 3 shows the temperature dependence of entropy compared to experimental results [50], which also demonstrate good agreement.

Thus, the crystal structure simulations successfully reproduced the temperature dependences of heat capacity and entropy, showing reasonable agreement with available experimental data. Furthermore, they enabled reliable extrapolation of these thermodynamic properties to higher temperature ranges.

## CONCLUSION

The empirical interatomic potential method was used to model $ZnWO_4$ crystals. The lattice parameters, atomic coordinates, interatomic distances, elastic constants and moduli, and temperature dependencies of heat capacity and entropy were evaluated. In most cases, the obtained results are consistent with and complement existing literature data. The developed system of interatomic potentials enables simulations of more complex composite media, solid solutions containing $ZnWO_4$, as well as for identifying compositions with optimized properties.

## FUNDING

This work was supported by Lomonosov Moscow State University within state budget theme No. AAAA-A16-116033010121-7. Part of the work was carried out within the framework of topic No. 124022400142-2 of the state assignment of the Institute of Geology of Ore Deposits, Petrography, Mineralogy and Geochemistry of the Russian Academy of Sciences. No additional grants to carry out or direct this particular research were obtained.

## CONFLICT OF INTERESTS

The authors of this work declare that they have no conflicts of interest.

## REFERENCES

1. *Kroeger E.A.* // Some Aspects of the Luminescence of Solids. New York: Elsevier, 1948. P. 107.
2. *Degoda V.Ya., Afanasieva L.A., Belli P. et al.* // J. Lumin. 2022. V. 249. 119028. https://doi.org/10.1016/j.jlumin.2022.119028
3. *Nagornaya L.L., Dubovik A.M., Vostretsov Y.Y.* // IEEE Trans. Nucl. Sci. 2008. V. 55. P. 1469. https://doi.org/10.1109/TNS.2007.910974
4. *Galashov E.N., Gusev V.A., Shlegel V.N., Vasiliev Ya.V.* // Crystallography Reports. 2009. V. 54. P. 689. https://doi.org/10.1134/S1063774509040245
5. *Leng X., Dai L., Chao X. et al.* // Optik. 2014. V. 125. P. 1267. http://dx.doi.org/10.1016/j.ijleo.2013.08.033
6. *Atuchin V.V., Bekenev V.L., Borovlev Yu.A. et al.* // J. Optoelectron. Adv. Mater. 2017. V. 19. P. 86.
7. *Barabash A.S., Belli P., Bernabei R. et al.* // Nucl. Instrum. Methods Phys. Res. A. 2016. V. 833. P. 77. http://dx.doi.org/10.1016/j.nima.2016.07.025
8. *Belli P., Bernabei R., Borovlev Y.A. et al.* // Nucl. Instrum. Methods Phys. Res. A. 2022. V. 1029. 166400. https://doi.org/10.1016/j.nima.2022.166400
9. *Grassmann H., Moser H.G.* // J. Lumin. 1985. V. 33. P. 109. https://doi.org/10.1016/0022-2313(85)90034-1
10. *Dkhilalli F., Borchani S.M., Rasheed M.* // J. Mater. Sci.: Mater. Electron. 2018. V. 29. P. 6297. https://doi.org/10.1007/s10854-018-8609-z
11. *Jeong H.Y., Lim H.S., Lee J.H.* // Nanomaterials. 2020. V. 10. P. 1721. http://dx.doi.org/10.3390/nano10091721
12. *De Macedo O.B., de Oliveira A.L.M., dos Santos I.M.G.* // Ceramica. 2022. V. 68. P. 294. https://orcid.org/0000-0002-7930-6234
13. *Lou Z., Hao J., Cocivera M.* // J. Lumin. 2002. V. 99. P. 349. https://doi.org/10.1016/S0022-2313(02)00372-1

14. *Bernabei R., Belli P., Cappella F. et al.* // EPJ Web Conf. 2017. V. 136. 05002. https://doi.org/10.1051/epjconf/201713605002
15. *Caracciolo V., Degoda V.Ya., Belli P. et al.* // SciPost Phys. Proc. 2023. V. 12. P. 021. https://doi.org/10.21468/SciPostPhysProc.12.021
16. *Wang X., Fan Z., Yu H. et al.* // Opt. Mater. Express. 2017. V. 7. P. 1732. https://doi.org/10.1364/OME.7.001732
17. *Xia Z., Yang F., Qiao L., Yan F.* // Opt. Commun. 2017. V. 387. P. 357. http://dx.doi.org/10.1016/j.optcom.2016.12.008
18. *Subbotin K., Loiko P., Volokitina A. et al.* // J. Lumin. 2020. V. 228. 117601. https://doi.org/10.1016/j.jlumin.2020.117601
19. *Chen X.P., Xiao F., Ye S. et al.* // J. Alloys Compd. 2011. V. 509. P. 1355. https://doi.org/10.1016/j.jallcom.2010.10.061
20. *Ran W., Wang Q., Zhou Y. et al.* // Mater. Res. Bull. 2015. V. 64. P. 146. http://dx.doi.org/10.1016/j.materresbull.2014.12.050
21. *Filipenko O.S., Pobedimskaya E.A., Belov N.V.* // Kristallografiya. 1968. V. 13. P. 163.
22. *Trots D.M., Senyshyn A., Vasylechko L. et al.* // J. Phys.: Condens. Matter. 2009. V. 21. 325402. https://doi.org/10.1088/0953-8984/21/32/325402
23. *Brik M.G., Nagirnyi V., Kirm M.* // Mater. Chem. Phys. 2013. V. 137. P. 977. http://dx.doi.org/10.1016/j.matchemphys.2012.11.011
24. *Zhang X.Q., Zhang B.* // Rus. J. Phys. Chem. B. 2023. V. 17. P. 1049. http://dx.doi.org/0.1134/S1990793123050135
25. *Errandonea D., Manjón F.J., Garro N. et al.* // Phys. Rev. B. 2008. V. 78. 054116. http://dx.doi.org/10.1103/PhysRevB.78.054116
26. *Evarestov R., Kalinko A., Kuzmin A. et al.* // Integr. Ferroelectr. 2009. V. 108. P. 1. https://doi.org/10.1080/10584580903323990
27. *Kohn W., Sham L.J.* // Phys. Rev. 1965. V. 140. P. A1133. https://doi.org/10.1103/PhysRev.140.A1133
28. *Perdew J.P., Chevary J.A., Vosko S.H. et al.* // Phys. Rev. B. 1992. V. 46. P. 6671. https://doi.org/10.1103/PhysRevB.46.6671
29. *Perdew J.P., Burke K., Ernzerhof M.* // Phys. Rev. Lett. 1996. V. 77. P. 3865. https://doi.org/10.1103/PhysRevLett.77.3865
30. *Senyshyn A., Kraus H., Mikhailik V.B., Yakovyna V.* // Phys. Rev. B. 2004. V. 70. 214306. https://doi.org/10.1103/PhysRevB.70.214306
31. *Dudnikova V.B., Zharikov E.V.* // Phys. Solid State. 2017. V. 59. P. 866 http://dx.doi.org/10.1134/S1063783417050110
32. *Lin Q., Feng X* // J. Phys.: Condens. Matter. 2003. V. 15. P. 1963. http://dx.doi.org/10.1088/0953-8984/15/12/313
33. *Dudnikova V.B., Zharikov E.V., Eremin N.N.* // Mater. Today Commun. 2020. V. 23. 101180. http://doi.org/10.1016/j.mtcomm.2020.101180
34. *Shao Z., Zhang Q., Liu T., Chen J.* // Nucl. Instrum. Methods Phys. Res. B. 2008. V. 266. P. 797. http://dx.doi.org/10.1016/j.nimb.2008.01.018
35. *Dudnikova V.B., Zharikov E.V., Antonov D.I., Eremin N.N.* // Phys. Solid State. 2022. V. 64. P. 1713. https://doi.org/10.21883/pss.2022.11.54195.413
36. *Huang H., Liu L., Tian N., Zhang Y.* // J. Alloys Compd. 2015. V. 637. P. 471. http://dx.doi.org/10.1016/j.jallcom.2015.02.224
37. *Tang L., Zhu M., Chen W. et al.* // New J. Chem. 2020. V. 44. P. 19796. http://dx.doi.org/10.1039/d0nj04622a
38. *Malyukin Y., Seminko V., Maksimchuk P., Bespalova I.* // Opt. Mater. 2019. V. 98. 109455. https://doi.org/10.1016/j.optmat.2019.109455
39. *Krutyak N., Nagirnyi V., Zadneprovski B., Buriy M.* // J. Lumin. 2024. V. 267. 120356. https://doi.org/10.1016/j.jlumin.2023.120356
40. *Gale J.D.* // Z. Kristallogr. 2005. V. 220. P. 552. https://doi.org/10.1524/zkri.220.5.552.65070
41. *Urusov V.S., Eremin N.N.* Atomistic computer simulation of the structure and properties of inorganic crystals and minerals, their defects and solid solutions. M. GEOS. 2012. 428 p.
42. *Scofield P.F., Knight K.S., Redfern S.A.T., Cressey G.* // Acta Cryst. B. 1997. V. 53. P. 102. https://doi.org/10.1107/S0108767396008446
43. *Dahlborg M.A., Svensson G.* // Acta Chem. Scandinavica. 1999. V. 53. P. 1103. https://doi.org/10.3891/acta.chem.scand.53-1103
44. *Redfern S.A.T., Bell A.M.T., Henderson C.M.B. et al.* // Eur. J. Mineral. 1995. V. 7. P. 1019. https://doi.org/10.1127/ejm/7/4/1019
45. *Kuzmin A., Purans J.* // Radiat. Measur. 2001. V. 33. P. 583. https://doi.org/10.1016/S1350-4487(01)00063-4
46. *Yadav P., Rout S.K., Sinha E.* // J. Alloys Compd. 2017. V. 726. P. 1014. http://dx.doi.org/10.1016/j.jallcom.2017.07.308
47. *Pisarevskii Yu.V., Silvestrova I.M., Voszka R. et al.* // Phys. Status Solidi. A. 1988. V. 107. P. 161. https://doi.org/10.1002/pssa.2211070115
48. *Ruiz-Fuertes J., Lopez-Moreno S., Errandonea D. et al.* // J. Appl. Phys. 2010. V. 107. 083506. http://dx.doi.org/10.1063/1.3380848
49. *Ma L., Yibibulla T., Jiang Y. et al.* // Physica E. 2022. V. 136. 114990. https://doi.org/10.1016/j.physe.2021.114990
50. *Lyon W.G., Westrum Jr. E.F.* // J. Chem. Thermodyn. 1974. V. 6. P. 763. https://doi.org/10.1016/0021-9614(74)90141-4
51. *Landee C.P., Westrum Jr. E.F.* // J. Chem. Thermodyn. 1975. V. 7. P. 973. https://doi.org/10.1016/0021-9614(75)90161-5
52. *Popov P.A., Skrobov S.A., Matovnikov A.V. et al.* // Phys. Solid State. 2016. V. 58. P. 853. https://doi.org/10.1134/S1063783416040193